Transactions of the **14th International Conference on Structural Mechanics in Reactor Technology** (SMiRT 14), Lyon, France, August 17-22, 1997 **L02/2**

Experimental study of the cyclic behaviour of a stainless steel under complex multiaxial loadings in tension-torsion-internal and external pressure

Bocher L., Delobelle P.
Faculté des Sciences de Besançon, France

ABSTRACT. This paper is concerned with the experimental behaviour of a 316 stainless steel at room temperature and under non proportional cyclic strainings in tension-torsion-internal and external pressures. The two or three sinusoïdal strains were applied both in and out-of-phase and the main investigations deal with the additional hardening due to multiaxiality of the loadings. With respect to the increasing maximum additional hardening, the different tests can be classified as follows : in-phase tests, out-of-phase internal-external pressure tests, out-of-phase tension-torsion tests and finally tension-torsion-pressure tests with significant phase angles.

I - INTRODUCTION

The availability of commercial hydraulic tensile-torsion machines over the last fifteen years has lead to the important development of experimental studies on the behaviour of materials under biaxial cyclic loadings [1-10]. Paradoxically, exept in the case of pure fatigue, [11-12], very few studies have been performed with a cyclic component in internal and external pressures. This observation is certainly due to the fact that there are no off-the-shelf hydraulic machines commercially available allowing this type of loading to be performed. To overcome this barrier, we have designed and constructed a medium pressure chamber allowing the specimen to be confined and which is adapted to a tensile-torsion machine. The addition of an independent hydraulic system allows the realization of triaxial cyclic tests in tensile-torsion and in internal-external pressures. This type of tests is now completely controlled.

From the point of view of materials, in the case of austenitic stainless steels [4] [6-10], it has been shown that a very strong supplementary hardening appears under tensile-torsion biaxial cyclic loadings which is directly related to the phase shift between the strain components and to the ratio between the maximal amplitude of these components. This supplementary hardening is a fairly strong decreasing function of the temperature [7,9]. In the present study, performed at room temperature, we propose to analyse qualitatively and quantitatively the effect on the tension-torsion behaviours in the case of tension-pressure and tension-torsion-pressure where these components are out-of-phase with one another. It is important to notice that it is a first study of this type and as a consequence, the results obtained will have to be confirmed by other experiments. A fairly exhaustive study under this type of loading is currently being performed and will allow the set of mechanical parameters influencing the supplementary hardening to be analysed.

II - EXPERIMENTAL METHODS

II.1 Specimens and mechanical dimensions

The specimens are obtained from slices taken from a sheet metal 30 mm wide, hyper-quenched from 1.200°C. The micro-structure is entirely austenitic and the average diameter of the grains is about 45 μm. The weight composition of this controlled low-carbon and nitrogen 17-12 Mo SPH steel is given in Table I.

Table I - Chemical composition of the studied stainless steel (weight %)

C	S	P	Si	Mn	Ni	Cr	Mo	N	B
≤ 0.03	≤ 0.001	≤ 0.021	≤ 0.44	1.084	12.3	17.54	2.47	0.075	0.001

Co	Cu	Ti	Nb	Al	Ta	Fe
0.15	0.175	≤ 0.005	0.015	0.10	-	bal.

Given the types of loading to be performed, the specimens have a tubular shape with sufficiently thin walls to assume that the stresses as homogeneous for a given radius. Thus, the exterior and interior diameters of the specimens are respectively of 16 mm and 14 mm with a gage length of 20 mm of which only the central 10 mm are used for the extensometry. The total length of the specimen is 113 mm. The entire geometry of the specimen has been validated by an elastic finite element calculation. The stress-tensor for a test in tensile-torsion-pressure is written :

$$\underline{\sigma} = \begin{bmatrix} \sigma_{zz} & \sigma_{z\theta} & 0 \\ \sigma_{z\theta} & \sigma_{\theta\theta} & 0 \\ 0 & 0 & \sigma_{rr} \end{bmatrix} \text{ with } \left\{ \begin{array}{l} \sigma_{zz} = \dfrac{F}{\pi(r_2^2 - r_1^2)} + \dfrac{1}{2}\dfrac{(P_1 r_1 - P_2 r_2)}{(r_2 - r_1)}, \sigma_{\theta\theta} = \dfrac{P_1 r_1 - P_2 r_2}{r_2 - r_1} \\ \sigma_{rr} = -\dfrac{P_1 + P_2}{2} \text{ and } \sigma_{z\theta} = \dfrac{3C}{2\pi(r_2^3 - r_1^3)} \end{array} \right\} \quad (1).$$

(r, θ, z) is a cylindrical coordinate system with the z axis oriented along the specimen axis. In these equations, F is the value of the force read by the cell, C the torque exerted at one extremity of the tube and P_1, P_2 respectively the applied pressures on internal (radius r_1) and external (radius r_2) surfaces of the specimen. These equations are derived with the hypothesis of thin-walled tubes, which leads to errors on the stress components lower than 10 %.

As for the strain measurements, the confinement of the specimen does not allow the use of classical mechanical extensometers, as in the case of a single torsion-internal pressure test. The strain gauges are thus glued and a few additional precautions are necessary in the context of the experiments. The application of a significant hydrostatic pressure can change the response of the gauges, the effect of a transversal contraction of the gauges can be significative and the shear strain provokes a slight rotation. Moreover, since the gauges only measure the strains along their directions, it is necessary to carefully select their positions on the specimen so that the decoupling between the strains be as simple as possible given that the test machine is directly controlled by these strains. Toward this end, we chose a 45° rosette composed of three gauges respectively orientated about the circonference $\alpha = 0°$, at $\alpha = 45°$ and $\alpha = 90°$ from this direction, which leads directly ε_{zz} ($\alpha = 0°$), $\varepsilon_{\theta\theta}$ ($\alpha = 90°$) and $\varepsilon_{z\theta} = \varepsilon$ ($\alpha = 45°$) - $1/2(\varepsilon_{zz} + \varepsilon_{\theta\theta})$ for $\alpha = 45°$. Since the machine is controlled by these three strains, the calculation of the shear component has to be performed in real time from signals transmitted by the three gauges. This operation is performed with a small electronic calculator with analogical operators. In order to perform the multiaxial experiments at comparable total strains amplitudes and to analyse the results of these tests, equivalent stress and strain values are used :

$$\bar{\sigma} = \sqrt{3/2}\,(\sigma'_{ij}\sigma'_{ij})^{1/2} = (\sigma_{zz}^2 + \sigma_{\theta\theta}^2 + \sigma_{rr}^2 - \sigma_{zz}\sigma_{\theta\theta} - \sigma_{zz}\sigma_{rr} - \sigma_{\theta\theta}\sigma_{rr} + 3\sigma_{z\theta}^2)^{1/2}$$
$$\bar{\varepsilon} = \sqrt{2/3}\,(\varepsilon_{ij}\varepsilon_{ij})^{1/2} = (2/\sqrt{3})(\varepsilon_{zz}^2 + \varepsilon_{\theta\theta}^2 + \varepsilon_{zz}\varepsilon_{\theta\theta} + \varepsilon_{z\theta}^2)^{1/2} \quad (2).$$

II.2 The experimental set up

All the tests have been performed on a Schenk hydraulic tensile-torsion machine. This machine can be piloted either in force, torque, or in strains. The test instructions are delivered by a PC HP 308 which by communicating with a central acquisition system HP 3852A allows two outputs to be generated for all types of desired signals. This basic installation has been modified in order to apply an alternating circonferential stress. Two independent super-pressure blocks have been added which multiply the pressure by four and are able to generate maximal pressures of up to 1000 bars. One is used to apply a pressure on the internal wall of the tube and the other on the external wall. These two super-pressures devices can be commanded separatedly in the case of a pressure control or else coupled in the case of strain control.

For the confinement device, we have retained the solution whereby the chamber is directly guided by the specimen and where the pressure seal is assured at the guide interface. This solution allows us to have a relatively small chamber size which is preferable in the case of high pressures. The specimen fixation at the jaws is assured by two threaded extensions added and welded to the extremities of the specimen.

III - THE MULTIAXIAL CYCLIC TESTS. RESULTS AND ANALYSIS

III.1 Test presentation

The behavior of this type of stainless steel under uni and bidirectional loading in tension-torsion has been very thoroughly studied at ambiant temperature [4] [6-10] which allows, given a few calibrations and verification tests, to establish a reliable and complete experimental basis for these two types of loadings. These classical tests will not be examined here. The tests presented below consist in the application and control of either two strains $\varepsilon_{zz}^T, \varepsilon_{\theta\theta}^T$ or three strains $\varepsilon_{zz}^T, \varepsilon_{\theta\theta}^T$ and $\varepsilon_{z\theta}^T$. Superscipt T denotes total values.

Before continuing, it is important to specify the exact nature of these tests. The three controlled components are planar and, as we have seen above, the resultant stresses are tri-dimensional (Eq. 1). We can thus speak of tri-axial tests in the strict sense of the word. However, it is true that σ_{rr} is small in comparison with the other components and that it intervenes more as a parasitic stress than as a test parameter. The three imposed signals have the form :

$$\varepsilon_{zz}^T = \varepsilon_{zzM}^T \sin\omega t\,,\ \varepsilon_{\theta\theta}^T = \varepsilon_{\theta\theta M}^T \sin(\omega t - \varphi)\,,\ \varepsilon_{z\theta}^T = \varepsilon_{z\theta M}^T(\sin\omega t - \delta) \quad (3)$$

The values of $\varepsilon_{zzM}^T, \varepsilon_{\theta\theta M}^T$ and $\varepsilon_{z\theta M}^T$ condition the importance of each one of these components and φ, δ set the phase shift between them. In the general case of the tension-torsion-pressure loadings, each one of these maximal components express themselves as a function of the maximal equivalent von Mises strain, $\bar{\varepsilon}_M^T$ (Eq. 2), namely :

$$\varepsilon_{zzM}^T = \frac{\sqrt{3/2}\,\bar{\varepsilon}_M^T}{\sqrt{A - \sqrt{B+C}}}, \varepsilon_{z\theta M}^T = r_2\frac{\sqrt{3}}{2}\varepsilon_{zzM}^T, \varepsilon_{\theta\theta M}^T = r_1\varepsilon_{zzM}^T \text{ with } A = 1 + r_1^2 + \frac{3}{4}r_2^2 + r_1\cos\varphi,$$
$$B = \left(\frac{3}{4}r_2^2\sin 2\delta + r_1\sin\varphi + r_1^2\sin 2\varphi\right)^2 \text{ and } C = \left(1 + \frac{3}{4}r_2^2\cos 2\delta + r_1\cos\varphi + r_1^2\cos 2\varphi\right)^2 \quad (4)$$

In this way, working with $\bar{\varepsilon}_M^T$ fixed, it is possible to calculate, using Eq. 4, the three amplitudes ε_{zzM}^T, $\varepsilon_{\theta\theta M}^T$ and $\varepsilon_{z\theta M}^T$ for r_2, r_1, φ and δ imposed. Since the experimental basis in tension, torsion and tension-torsion is available, we only present the tests in tension-pressure in phase and out-of-phase as well as the tests of tensile-torsion-pressures with just three components in phase, then two and a test where all three components are phase shifted. In this study, all of the tests have amplitude ratios which are fixed, namely $r_1 = \pm 1$ and $r_2 = 1$. The possible trajectories are shown in Fig. 1 for different values of φ and δ in the von Mises planes. For the tension-pressure test, in order to cover all the possibilities, the angle φ must vary between 0° and 180° with $r_1 = 1$. However, as soon as $\varphi > 90°$ with $r_1 = 1$, the equivalent strain in the first quarter cycle is greater than the desired value. This difficulty is avoided by adopting a ratio $r_1 = -1$ an by fixing a new phase shift angle such that $[\varphi(r_1 = -1) = \pi - \varphi(r_1 = 1)$. The only difference with the situation $\varphi < 90°$ is the rotation direction of the trajectory. For the seven performed test whose loading characteristics are given in Table II, we impose $\bar{\varepsilon}_M^T = 0.4\ \%$, $\omega = 1.88\ 10^{-2} s^{-1}$ and $r_1 = \pm 1$, $r_2 = 1$. On each specimen, several incremental or decremental phase shifts are imposed. For each pair of phase shift values, 50 cycles are performed. This value seems sufficient in order to reach the stabilized cycle corresponding to this pair, at least for the incremental procedure.

Table II - Tension-Torsion-Internal, External Pressure Tests

Test 1, Sequence	$r_1 = 1$ $\varphi = 0°$ (1) → $\varphi = 60°$ (2) → $\varphi = 90°$ (3)
Test 2, Sequence	$r_1 = 1$ $\varphi = 90°$ (23) → $\varphi = 60°$ (-) → $\varphi = 0°$ (-)
Test 3, Sequence	$r_1 = -1$ $\varphi = 0°$ (4) → $\varphi = 30°$ (5) → $\varphi = 60°$ (6)
Test 4, Sequence	$r_1 = -1$ $\varphi = 60°$ (24) → $\varphi = 30°$ (-) → $\varphi = 0°$ (-)
Test 5, Sequence	$r_1 = r_2 = 1$ $\varphi = \delta = 0°$(7) → $\varphi = 0°, \delta = 60°$(8) → $\varphi = 0°, \delta = 90°$(9) → $\varphi = 0°, \delta = 0°$(-)
Test 6 , Sequence	$r_2 = 1$; $r_1 = 1$ $\varphi = \delta = 0°$(10) → $r_1 = 1, \delta = 0°$, $\varphi = 60°$(11) → $r_1 = 1, \delta = 0°$, $\varphi = 90°$(12) → $r_2 = 1$; $r_1 = -1, \delta = 0°$, $\varphi = 60°$(13) → $r_1 = -1, \delta = 0°$, $\varphi = 30°$(-) → $r_1 = 1, \delta = 0°$, $\varphi = 0°$(-0)
Test 7, Sequence	$r_2 = 1; r_1 = 1$, $\delta = \varphi = 0°$(14) → $r_1 = 1$, $\delta = 0°$, $\varphi = 30°$(15) → $r_1 = 1$, $\delta = 60°, \varphi = 30°$(16) → $r_2 = 1; r_1 = 1, \delta = 90°, \varphi = 30°$(17) → $r_1 = 1, \delta = 100°, \varphi = 30°$(18) → $r_1 = -1, \delta = 0°, \varphi = 60°$(19) → $r_2 = 1; r_1 = -1, \delta = 60°, \varphi = 60°$(20) → $r_1 = -1, \delta = 90°, \varphi = 60°$(21) → $r_1 = -1, \delta = 41.4°, \varphi = 82.8°$(22)

III.2 Tests results

For each test and in accordance with each phase shift, it is possible to calculate and to represent each one of the loops $\sigma_{ij} = f(\varepsilon_{ij}^T)$, the stress and plastic strain paths in the von Mises planes $\sigma_{ij} = f(\sigma_{kl})$, $\varepsilon_{ij}^p = f(\varepsilon_{kl}^p)$, the evolution of the maximal von Mises stress $\bar{\sigma}_M$ and its equivalent in plastic strain $\bar{\varepsilon}_M^P$ as a function of the cycle number N_C.

Special attention should be given to Figure 2 corresponds to the test 1, sequence 1, $\varphi = 0°$, performed in tension-pressures. Indeed, the similitary between the cycles along the axial and circonferential directions shows that the determination of $\sigma_{\theta\theta}$ is correct and that the effect of pressure tight joint on the specimens can be considered as negligible during the translational motion of the specimen within the pressure chamber. The dissymetry with respect to the origin

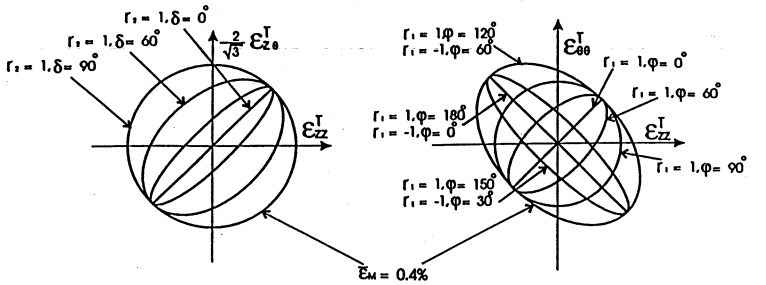

• Fig. 1 : Loading paths in the von Mises planes $\left(2/\sqrt{3}\,\varepsilon^T_{z\theta}, \varepsilon^T_{zz}\right)$ and $\left(\varepsilon^T_{\theta\theta}, \varepsilon^T_{zz}\right)$.

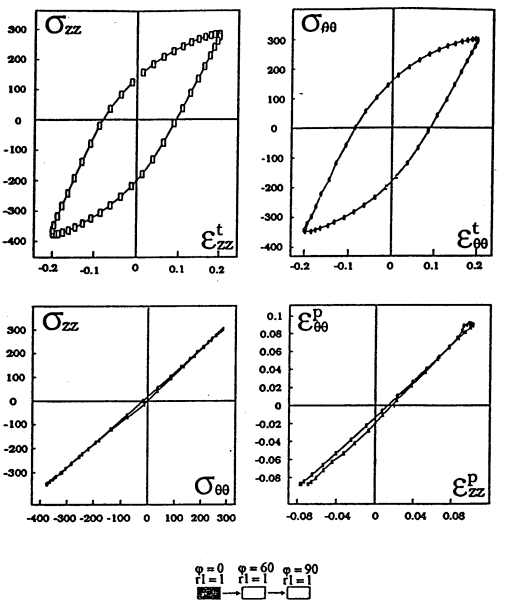

• Fig. 2 : Responses at the stabilized cycle of Test n° 1, sequence 1, Table II : $r_2 = 0$, $r_1 = 1$ and $\varphi = 0°$.

• Fig. 3 : Evolution of $\bar{\sigma}_M$ as a function of the number of cycles N_c for the four tension-pressures tests - Tests 1, 2, 3 and 4, Table II .

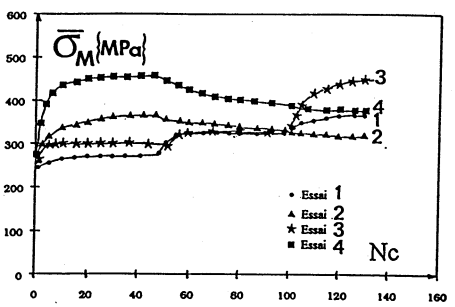

of the two loops, the latter being translated towards the botton, is due to the presence of the constantly negative component σ_r. Hence, the participation of σ_r is not negligible and it is therefore truly a triaxial test in the strictest sense of the term.

For the totality of tests 1 to 4, Fig. 3 shows the evolution of $\bar{\sigma}_M$ as a function of the number of cycles N_C. The maximal hardening is obtained for $r_1 = -1$, $\varphi = 60°$. However, it is important to notice that this loading corresponds to the amplitude of the maximal plastic strain which distorts the comparison with the other sequences. We will return to this point later during the analysis of the set of results. For the tests 5 and 6 (Table II), two of the three components are in phase, the third being phase shifted $\varepsilon^T_{z\theta}(\delta), \varepsilon^T_{\theta\theta}(\varphi)$. For the test 7, the three components are phase shifted, according to a fairly complicated sequence which should lead to a constantly increasing hardening. Fig. 4 gives an example of the loops obtained during the test 7, sequence 3 and Fig. 5 shows the evolution of $\bar{\sigma}_M$ as a function of N_C for these three tests. The maximum hardening correspond to $\delta = 90°$, $r_1 = 1$ for $\varphi = 0$, $r_2 = 1$ (test 5), a result which is identical to that of tension-torsion, $\varphi = 60°$, $r_1 = -1$ for $\delta = 0$, $r_2 = 1$ (test 6), a result which is in accordance with the one presented before in tension-pressure only, and finally, $\varphi = 82.8°$, $r_1 = -1$ for $\delta = 41.4°$, $r_2 = 1$ in the general case.

III.3 Analysis of the results

In order to be able to perform a qualitative analysis of the totality of these tests, the maximal equivalent stress $\bar{\sigma}_M$ as well as the maximal plastic strain $\bar{\varepsilon}^P_M$ are calculated numerically and for each one of the sequences identified in Table II. The set of the calculated pairs $(\bar{\sigma}_M, \bar{\varepsilon}^P_M)$ are identified by their sequence number and reported in Fig. 6. Reference points from the literature obtained in tension-compression, alternating torsion, tension-torsion in and out-of-phase ($\delta = 90°$) are also reported on this figure. Hence forth, it is possible to trace fairly precisely the two relative reference lines, resulting from uniaxial cyclical tests or biaxial in-phase tension-torsion tests (curve 1) and to the tests of out-of-phase tension-torsion (curve 2). This figure allows the different types of loading to be classified with respect to the supplementary hardening. This classification is established as follows :

- The in-phase tests with two or three components ($\delta = \varphi = 0°$) : non supplementary hardening, curve 1, Fig. 6.
- The tension-pressure tests such as $r_1 = 1$, $\varphi = 90°$ and $r_1 = -1$, $\varphi = 60°$, the hardening is slightly lower than that of tension-torsion tests, curve 3, Fig. 6.
- The tension-torsion tests such as $r_2 = 1$, $\delta = 90°$, curve 2, Fig. 6.
- The tension-torsion-pressure tests where the three components are strongly shifted, namely : $r_1 = r_2 = 1$, $\delta = 90°$, $\varphi = 60°$ and $r_2 = 1$, $r_1 = -1$, $\delta = 41.4°$, $\varphi = 82.8°$, curve 4, Fig. 6. In this case the hardening is slightly greater than to the one recorded in tension-torsion.

This last observation corroborates those of Calloch et al [10] obtained in tension-torsion with butterfly paths. Note that a more thorough study is in preparation which considers all the possible combinations in tension-torsion-pressure and will be performed on the same material.

IV - CONCLUSIONS

A device is presented which allows cyclic tests to be performed on tubes for loadings in tension-torsion-internal and external pressures. Different tests have been performed at ambient temperature on an austenitic stainless steel which has the particularity of presenting a strong

supplementary hardening related to the non-radiality of the loadings. We study the influence of the phase shift parameters, namely the angle δ and φ for two or three cyclic sinusoidal components. The results are very rich in information and allow the different types of loading to be classified with respect to the observed supplementary hardening. The classification is established as follows :

- The in-phase tests with two or three components ($\delta = \varphi = 0°$) : no supplementary hardening.
- The tension-pressure tests such as $r_1 = 1$, $\varphi = 90°$ and $r_1 = -1$, $\varphi = 60°$.
- The tension-torsion tests such as $r_2 = 1$ and $\delta = 90°$.
- The tension-torsion-pressure tests where the three components are strongly shifted : $r_1 = r_2 = 1$, $\delta = 90°$ and $\varphi = 60°$ and $r_2 = 1$, $r_1 = -1$, $\delta = 41.4°$ and $\varphi = 82.8°$.

REFERENCES

1. Lamba H.S. and Sidebottom O.M., 1978, Cyclic plasticity for non proportional paths : Part I, cyclic hardening, erasure of memory and subsequent strain hardening experiments. J. Eng. Mat., vol. 100, 96-103
2. Brown M.W. and Miller K.J., 1979, Biaxial cyclic deformation behaviour of steels, Fat. Eng. Mat. and Struct., vol. 1, 93-106
3. Krempl E. and Lu H., 1984, The hardening and rate-dependent behavior of fully annealed AISI type 304 stainless steel under biaxial in-phase and out-of-phase strain cycling at room temperature, J. Eng. Mat. Techn., vol. 106, 376-382
4. Cailletaud G., Kaczmarek H. and Policella H., 1984, Some elements on multiaxial behavior of 316 steel at room temperature, Mech. Mat., vol. 3, 333-347
5. McDowell D.L., 1985, A two surface model for transient non proportional cyclic plasticity. Part I and II, J. Appl. Mech., vol. 52, 298-308
6. Benallal A. and Marquis D., 1987, Constitutive equations for non proportional cyclic elastoviscoplasticity, J. Eng. Mat. Techn., vol. 109, 326-336
7. Murakami S., Kawai M., Aoki K. and Ohmi Y., 1989, Temperature dependence of multi-axial non-proportional cyclic behaviour of type 316 stainless steel, J. Eng. Mat. Techn., vol. 111, 32-39
8. Delobelle P. and Lachat R., 1991, Viscoplastic properties and modeling of an austenitic stainless steel 17-12 SPH, at high temperature under in and out-of-phase cyclic tension-torsion loading, Rech. Aerosp., vol. 12, 21-37
9. Bouchou A. and Delobelle P., 1996, Behaviour and modelization of a 17-12 SPH stainless steel under cyclic, unidirectional and bidirectional anisothermal loadings, Nucl. Eng. Design, vol. 162, 21-45
10. Calloch S. and Marquis D., 1997, Additional hardening due to tension-torsion non-proportional loadings ; Influence of the loading path shape, Multiaxial Fatigue and Deformation Testing Techniques, ASTM STP 1280, 113-130
11. Fogue M., 1987, Critère de fatigue à longue durée de vie pour des états multiaxiaux de contraintes sinusoïdales en phase et hors phase, Thesis INSA Lyon
12. Vidal E., Kenmeugne B., Robert J.L. and Vahuaud J., 1996, Fatigue life prediction of components using multiaxial criteria, Mult. Fat. and Design. ESIS - Mech. Eng. Publ., 365-378

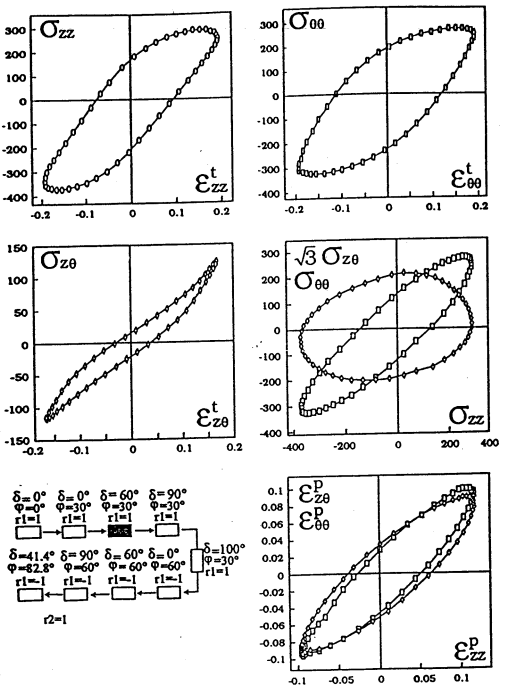

• Fig. 4 : Responses at the stabilized cycle of Test n° 7, sequence 16, Table II : $r_2 = 1$, $r_1 = 1$, $\delta = 60°$ and $\varphi = 30°$ $\left(\sigma_{zz} = f(\varepsilon^T_{zz}),\right.$ $\sigma_{\theta\theta} = f(\varepsilon^T_{\theta\theta})$, $\sigma_{z\theta} = f(\varepsilon^T_{z\theta})$, $\sqrt{3}\,\sigma_{z\theta}, \sigma_{\theta\theta} = f(\sigma_{zz})$ and $\left.\varepsilon^p_{z\theta}, \varepsilon^p_{\theta\theta} = f(\varepsilon^p_{zz})\right)$.

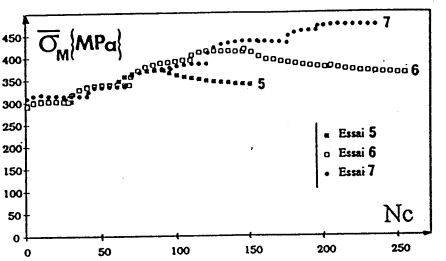

• Fig. 5 : Evolution of σ_M as a function of the number of cycles N_c for the three tension-torsion-pressures tests .

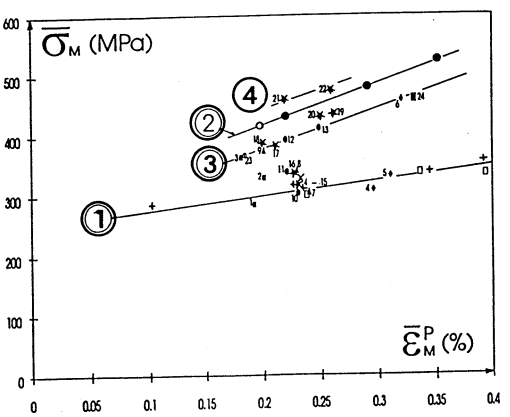

• Fig. 6 : $\bar{\sigma}_M$ versus $\bar{\varepsilon}^P_M$. Situation of the totality of the experimental points, Table II.

① in-phase test

② out-of-phasetension-torsion tests

③ out-of-phase tension-pressures tests

④ out-of-phase tension-torsion-pressures tests .